Supplement of Atmos. Chem. Phys., 17, 1453–1469, 2017
http://www.atmos-chem-phys.net/17/1453/2017/
doi:10.5194/acp-17-1453-2017-supplement

Supplement of

Real-time detection of highly oxidized organosulfates and BSOA marker compounds during the F-BEACh 2014 field study

Martin Brüggemann et al.

Correspondence to: Thorsten Hoffmann (t.hoffmann@uni-mainz.de)

S-1. UHPLC–(-)ESI–HRMS analysis of filter samples

S-1.1 Experimental details for the filter analysis

Filter samples were taken twice a day by passing an air flow of 27.5 L min^{-1} from ~6 m above ground ($PM_{2.5}$) through tetrafluorethylene-coated borosilicate filters (70 mm, Pallflex T60A20, Pall Life Science, USA). The sampling time was ~8 hours for daytime filters (9 a.m.–5 p.m.) and ~16 hours for nighttime filters (5 p.m.–9 a.m.). After sampling, the filters were stored at <-18 °C until analysis. Blank filters were taken every 2 to 3 days by placing a filter into the filter holder for ~20 min without sample flow.

For the extraction procedure one half of a filter sample was cut into pieces and 1.5 mL of a methanol/water solution (9:1) were added as extracting agent. Then, the sample was sonicated for 30 min. The extract was transferred into a separate glass vial and the filter sample extracted three more times in the same way. The combined extracts were then evaporated to dryness under a gentle stream of nitrogen at 50 °C. Afterwards, the residue was dissolved in 200 µL using a solution of acetonitrile/water (2:8). To compensate for losses during the sample processing, i.e. extraction efficiency and evaporation, an average recovery rate was determined for pinic acid, which served as a surrogate for the quantification of other monoterpene oxidation products. Here, an average recovery rate of 85% was found and applied to the detected organic compounds. It should also be noted that differences in extraction efficiencies and matrix effects might have had a significant effect on the observed signal abundances, which is an inherent problem for aerosol analysis by LC–MS, as recently discussed by Riva et al. (2016) for measurements of organosulfates from gas-phase oxidation of alkanes.

For the LC separation of the filter extracts a UHPLC system (Dionex UltiMate 3000, Thermo Scientific, Germany) equipped with a Hypersil Gold column (C18, 50x2.0 mm, 1.9 µm, Thermo Scientific, Germany) was used. The injection volume was 20 µL per run and each sample was measured in triplicate. As eluents served a solution of ultrapure water with 2% acetonitrile and 0.04% formic acid (eluent A) and a solution of acetonitrile with 2% of ultrapure water (eluent B). At a flow rate of 500 µL min^{-1} the following gradient was used to optimize the separation: 5% B at 0.00 min, 5% B at 0.50 min, 20% B at 1.00 min, 20% B at 1.50 min, 90% B at 2.00 min, 90% B at 4.00 min, 5% B at 4.05 min, and 5% B at 4.10 min. The UHPLC system was coupled to a Q-Exactive mass spectrometer (Thermo Scientific, Germany) which was used to obtain high resolution mass spectra (resolving power of $R=7\cdot10^4$ at m/z 200). Ionization of the LC eluent was carried out using electrospray ionization (ESI) in the negative mode with 40 psi sheath gas (N_2) and 20 psi aux gas (N_2). The capillary temperature was set to 350 °C and a potential of –3.0 kV was applied to the ESI needle. During each LC run the mass spectrometer operated in full scan mode with a scan range of m/z 80–550. Before running the measurements, the instrument was calibrated using the Pierce^{TM} calibration solution (Thermo Scientific, USA). For an accurate calibration of the lower mass range, butyric acid was added to the solution.

The obtained LC–MS data were recorded by XCalibur 2.2 (Thermo Scientific, USA) and further analyzed by Sieve 2.2 (Thermo Scientific, USA) which allowed a non-target screening of the obtained data set. The threshold for signal abundance was set to $2.5\cdot10^6$ a.u. (i.e signal to noise ratio ≥3) for the detection of significant signals in the obtained chromatograms after background subtraction by the software. For the elemental formula assignments, the following isotopes and conditions were used: ^{12}C (0–50), ^{1}H (0–100), ^{16}O (0–40), ^{14}N (0–4) and ^{32}S (0–4). The mass tolerance was set to ±5 ppm. Afterwards, the obtained compound list was checked for chemically unreasonable formula assignments, such as the absence of hydrogen in carbon-containing compounds or impossible O/C ratios ($O/C < 3$; $0.1 < H/C < 6$).

S-1.2 Detected signals and assigned compounds

Table S-1: List of CHO-containing compounds that were identified by UHPLC–(-)ESI–HRMS analysis of the filter samples.

formula for $[M–H]^-$	*m*/*z* for $[M–H]^-$	measured *m*/*z*	Δ*m* / ppm	Number of Oxygen	Number of Carbon	O:C
$C_4H_5O_5$	133.0142	133.0141	-1.1	5	4	1.3
$C_6H_7O_4$	143.0350	143.0349	-0.6	4	6	0.7
$C_6H_9O_4$	145.0506	145.0506	-0.2	4	6	0.7
$C_6H_9O_5$	161.0455	161.0454	-0.9	5	6	0.8
$C_6H_{13}O_6$	181.0718	181.0718	0.2	6	6	1.0
$C_6H_7O_7$	191.0197	191.0197	-0.1	7	6	1.2
$C_7H_9O_3$	141.0557	141.0557	-0.1	3	7	0.4
$C_7H_9O_4$	157.0506	157.0505	-0.9	4	7	0.6
$C_7H_{11}O_4$	159.0663	159.0661	-1.2	4	7	0.6
$C_7H_9O_5$	173.0455	173.0453	-1.4	5	7	0.7
$C_7H_{11}O_5$	175.0612	175.0611	-0.6	5	7	0.7
$C_7H_7O_6$	187.0248	187.0247	-0.6	6	7	0.9
$C_7H_9O_6$	189.0405	189.0403	-0.9	6	7	0.9
$C_8H_{13}O_3$	157.0870	157.0871	0.5	3	8	0.4
$C_8H_{11}O_4$	171.0663	171.0662	-0.5	4	8	0.5
$C_8H_{11}O_5$	187.0612	187.061	-1.1	5	8	0.6
$C_8H_{13}O_5$*	189.0768	189.0767	-0.8	5	8	0.6
$C_8H_9O_6$	201.0405	201.0403	-0.8	6	8	0.8
$C_8H_{11}O_6$*	203.0561	203.0561	-0.1	6	8	0.8
$C_9H_7O_4$	179.0350	179.0351	0.7	4	9	0.4
$C_9H_{13}O_4$	185.0819	185.0818	-0.7	4	9	0.4
$C_9H_{11}O_5$	199.0612	199.0612	0.0	5	9	0.6
$C_9H_{13}O_5$	201.0768	201.0768	-0.2	5	9	0.6
$C_9H_{15}O_5$	203.0925	203.0925	0.0	5	9	0.6
$C_9H_9O_6$	213.0405	213.0405	0.2	6	9	0.7
$C_9H_{11}O_6$	215.0561	215.0555	-2.9	6	9	0.7
$C_9H_{13}O_6$	217.0718	217.0716	-0.8	6	9	0.7
$C_9H_9O_7$	229.0354	229.0348	-2.5	7	9	0.8
$C_9H_{11}O_7$	231.0510	231.0505	-2.3	7	9	0.8
$C_{10}H_{15}O_3$	183.1027	183.1026	-0.4	3	10	0.3
$C_{10}H_{13}O_5$	213.0768	213.0768	-0.2	5	10	0.5
$C_{10}H_{15}O_5$	215.0925	215.0924	-0.5	5	10	0.5
$C_{10}H_{13}O_6$	229.0718	229.0715	-1.2	6	10	0.6
$C_{10}H_{15}O_6$	231.0874	231.0872	-0.9	6	10	0.6
$C_{10}H_{11}O_7$	243.0510	243.0506	-1.8	7	10	0.7

$C_{10}H_{15}O_7$	247.0823	247.0822	-0.5	7	10	0.7
$C_{11}H_{15}O_6$	243.0874	243.0873	-0.5	6	11	0.5
$C_{11}H_{17}O_6$*	245.1031	245.103	-0.3	6	11	0.5
$C_{12}H_{19}O_5$	243.1238	243.1237	-0.4	5	12	0.4
$C_{12}H_{21}O_5$	245.1394	245.1392	-1.0	5	12	0.4
$C_{13}H_{19}O_5$	255.1238	255.1239	0.4	5	13	0.4
$C_{13}H_{19}O_6$	271.1187	271.1188	0.3	6	13	0.5
$C_{14}H_{21}O_5$*	269.1394	269.1394	-0.2	5	14	0.4
$C_{17}H_{25}O_8$	357.1555	357.1559	1.1	8	17	0.5

*isobaric compounds detected

Table S-2: List of CHONS-containing compounds that were identified by UHPLC–(-)ESI–HRMS analysis of the filter samples.

formula for [M–H]$^-$	***m*/*z* for [M–H]$^-$**	**measured *m*/*z***	**Δ*m* / ppm**	**Number of Oxygen**	**Number of Carbon**	**O:C**
$C_5H_{10}O_9$NS	260.0082	260.0079	-1.1	9	5	1.8
$C_5H_9O_{11}N_2$S	304.9933	304.9932	-0.2	11	5	2.2
$C_6H_{10}O_9$NS	272.0082	272.0081	-0.3	9	6	1.5
$C_7H_{10}O_9$NS	284.0082	284.0080	-0.6	9	7	1.3
$C_7H_{10}O_{10}$NS	300.0031	300.0029	-0.6	10	7	1.4
$C_{10}H_{16}O_7$NS	294.0653	294.0657	1.4	7	10	0.7
$C_{10}H_{14}O_8$NS	308.0446	308.0448	0.8	8	10	0.8
$C_{10}H_{16}O_8$NS	310.0602	310.0605	0.9	8	10	0.8
$C_{10}H_{16}O_9$NS	326.0551	326.0551	-0.1	9	10	0.9
$C_{10}H_{16}O_{10}$NS	342.0500	342.0497	-1.0	10	10	1.0
$C_{10}H_{18}O_{10}$NS	344.0657	344.0655	-0.6	10	10	1.0
$C_{10}H_{17}O_{11}$N2S	373.0559	373.0558	-0.2	11	10	1.1
$C_{10}H_{15}O_{12}N_2$S	387.0351	387.0350	-0.3	12	10	1.2

Table S-3: List of CHON-containing compounds that were identified by UHPLC–(-)ESI–HRMS analysis of the filter samples.

formula for [M–H]$^-$	***m*/*z* for [M–H]$^-$**	**measured *m*/*z***	**Δ*m* / ppm**	**Number of Oxygen**	**Number of Carbon**	**O:C**
$C_7H_4O_5$N	182.0095	182.0096	0.6	5	7	0.7
$C_7H_3O_7N_2$	226.9946	226.9947	0.5	7	7	1.0
$C_{10}H_{16}O_8$N	278.0881	278.0882	0.2	8	10	0.8
$C_{11}H_{18}O_9$N	308.0987	308.0988	0.3	9	11	0.8

Table S-4: List of CHOS-containing compounds that were identified by UHPLC–(-)ESI–HRMS analysis of the filter samples.

formula for $[M–H]^-$	***m/z* for $[M–H]^-$**	**measured *m/z***	**Δm / ppm**	**Number of Oxygen**	**Number of Carbon**	**O:C**
$C_2H_3O_6S$	154.9656	154.9656	0.1	6	2	3.0
$C_3H_5O_6S$	168.9812	168.9812	-0.2	6	3	2.0
$C_4H_7O_6S$	182.9969	182.9967	-1.0	6	4	1.5
$C_5H_9O_6S$	197.0125	197.0124	-0.7	6	5	1.2
$C_5H_{11}O_6S$	199.0282	199.0280	-0.9	6	5	1.2
$C_5H_7O_7S$	210.9918	210.9916	-0.9	7	5	1.4
$C_5H_9O_7S$	213.0074	213.0075	0.2	7	5	1.4
$C_5H_{11}O_7S$	215.0231	215.0229	-0.9	7	5	1.4
$C_5H_7O_8S$	226.9867	226.9865	-0.9	8	5	1.6
$C_6H_{11}O_6S$	211.0282	211.0280	-0.9	6	6	1.0
$C_7H_{11}O_6S$	223.0282	223.0280	-0.8	6	7	0.9
$C_7H_{11}O_7S$	239.0231	239.0231	0.0	7	7	1.0
$C_7H_{13}O_7S$	241.0387	241.0385	-1.0	7	7	1.0
$C_7H_7O_8S$	250.9867	250.9868	0.3	8	7	1.1
$C_7H_9O_8S$	253.0024	253.0028	1.7	8	7	1.1
$C_8H_{13}O_7S$	253.0387	253.0384	-1.4	7	8	0.9
$C_8H_{11}O_9S$	283.0129	283.0127	-0.8	9	8	1.1
$C_8H_{13}O_9S$	285.0286	285.0284	-0.6	9	8	1.1
$C_8H_{13}O_{10}S$	301.0235	301.0231	-1.3	10	8	1.3
$C_9H_{15}O_6S$	251.0595	251.0593	-0.7	6	9	0.7
$C_9H_{15}O_7S$	267.0543	267.0543	0.0	7	9	0.8
$C_9H_{13}O_8S$	281.0337	281.0334	-0.9	8	9	0.9
$C_9H_{13}O_9S$	297.0286	297.0282	-1.3	9	9	1.0
$C_{10}H_{17}O_5S$	249.0802	249.0801	-0.5	5	10	0.5
$C_{10}H_{15}O_7S$	279.0544	279.0544	0.0	7	10	0.7
$C_{10}H_{17}O_7S$	281.0700	281.0698	-0.9	7	10	0.7
$C_{10}H_{17}O_8S$	297.0650	297.0646	-1.2	8	10	0.8
$C_{10}H_{15}O_9S$	311.0442	311.0440	-0.7	9	10	0.9
$C_{10}H_{17}O_9S$	313.0599	313.0596	-0.9	9	10	0.9
$C_{10}H_{15}O_{10}S$	327.0391	327.0387	-1.4	10	10	1.0
$C_{10}H_{13}O_{11}S$	341.0184	341.0183	-0.3	11	10	1.1
$C_{11}H_{19}O_7S$	295.0857	295.0858	0.3	7	11	0.6

S-2. Trajectory calculations for the campaign period

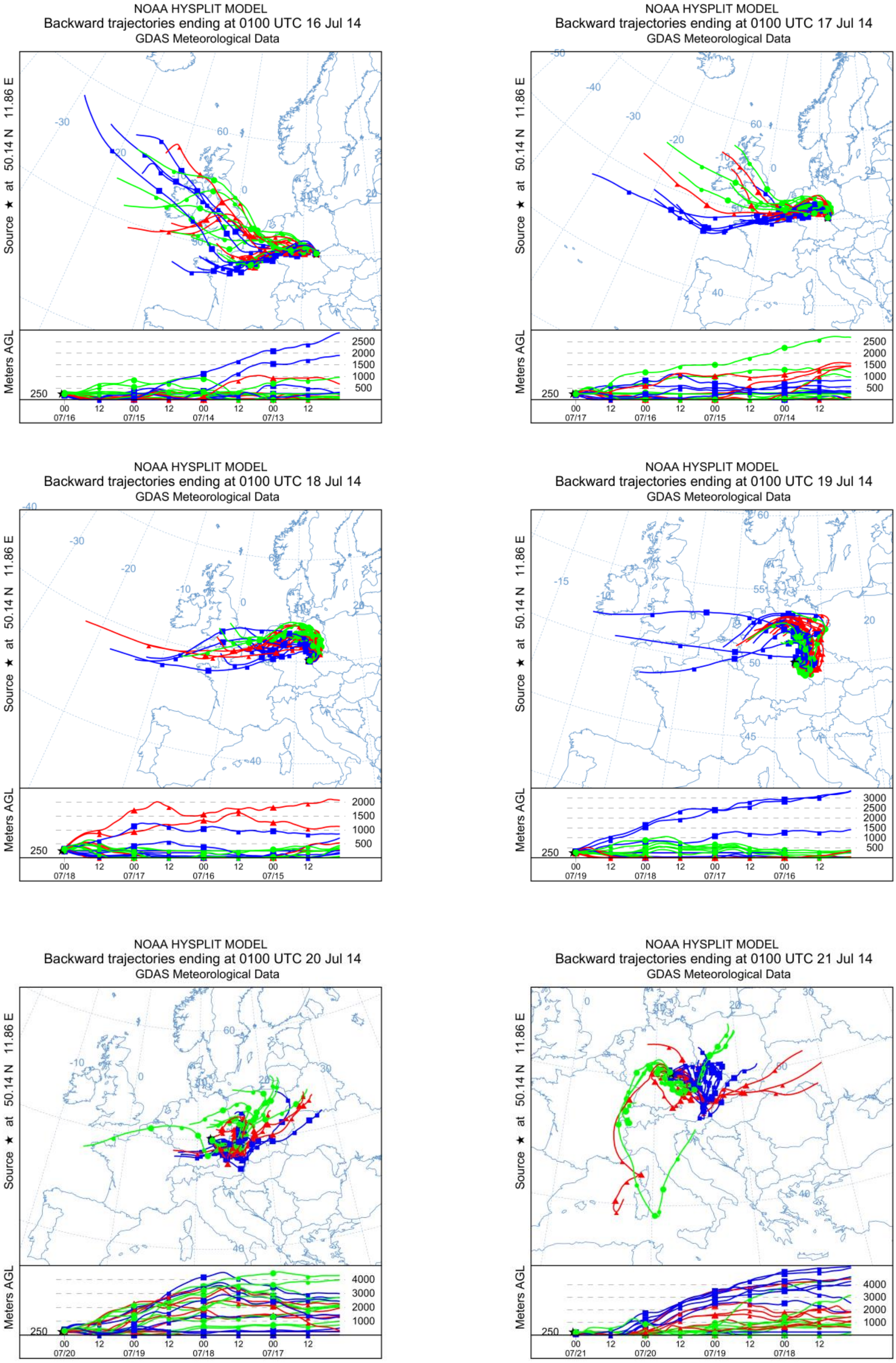

Figure S-1: 96 hours backward HYSPLIT trajectory calculations for the 16th-21st of July (each at 12 midnight CET) (Draxler and Rolph).

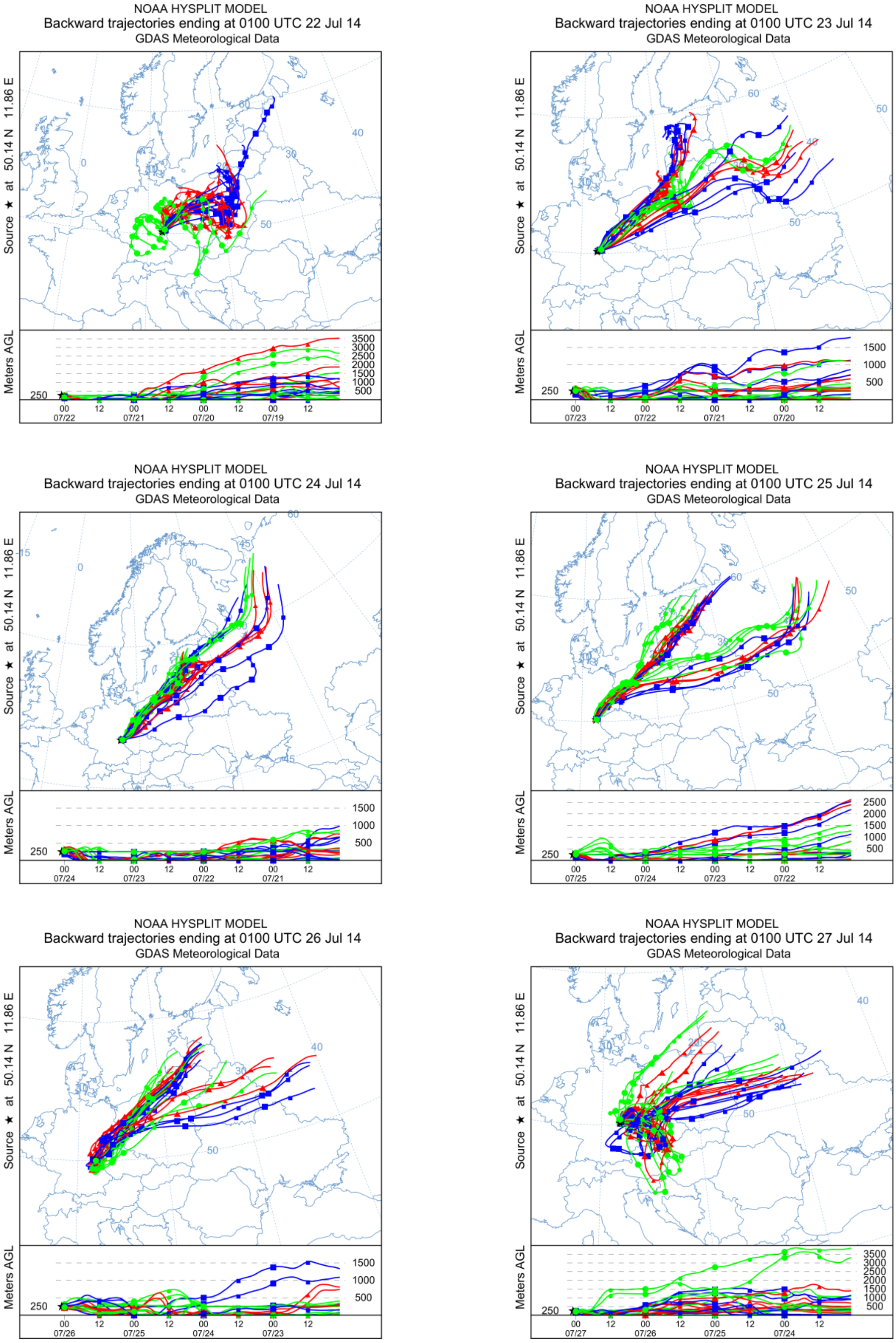

Figure S-2: 96 hours backward HYSPLIT trajectory calculations for the 22nd–27th of July (each at 12 midnight CET) (Draxler and Rolph).

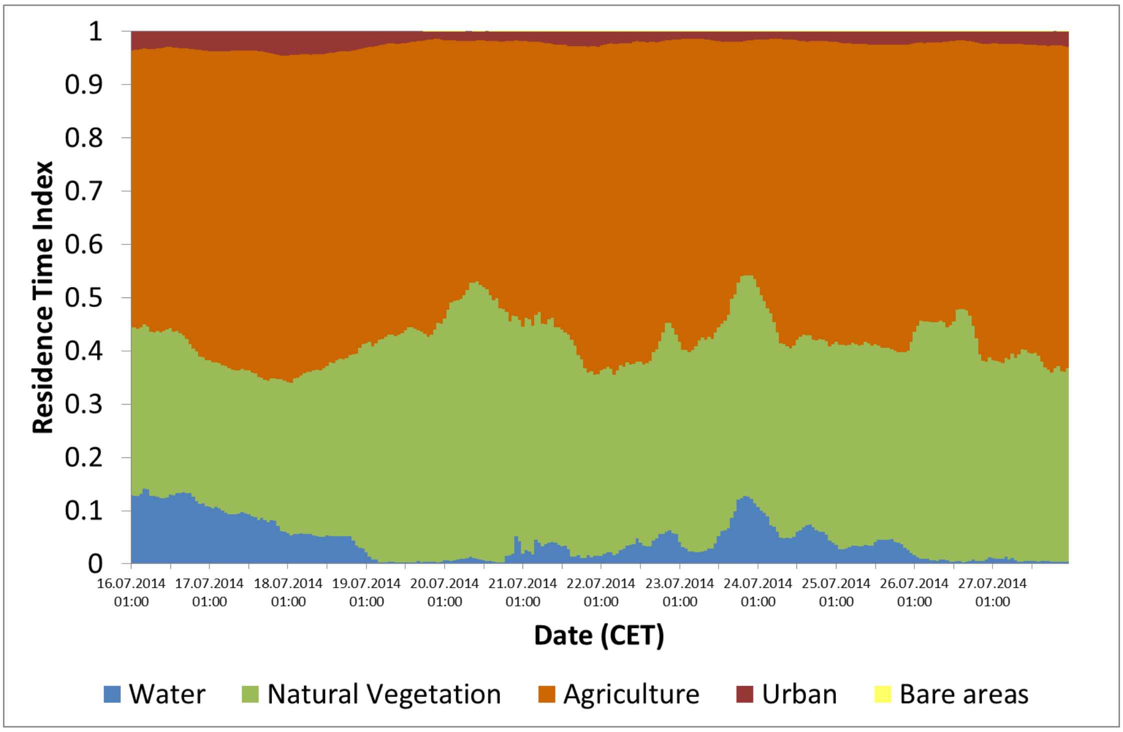

Figure S-3: Residence times for 96 hours backward trajectories arriving at the site intersected with satellite-derived global landcover data to give indications of influences of main land cover classes. A detailed description of the calculation method can be found elsewhere (van Pinxteren et al., 2010).

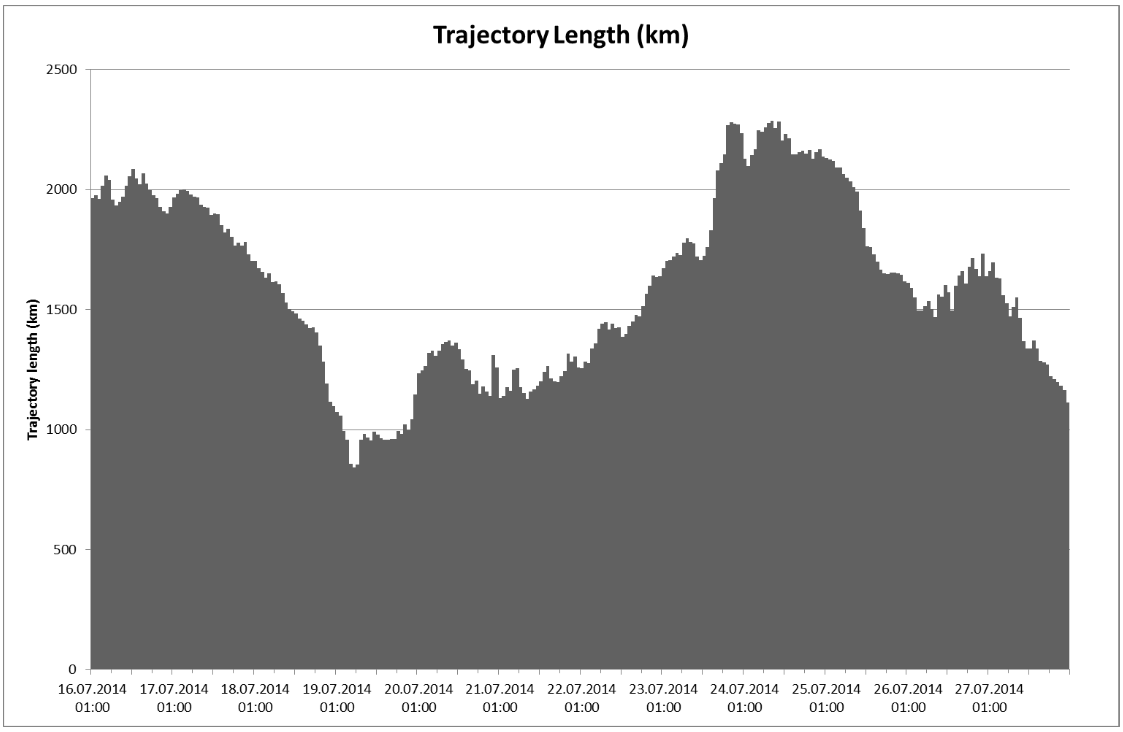

Figure S-4: Trajectory lengths for 96 hours backward trajectories arriving at the site. For details see van Pinxteren et al. (2010).

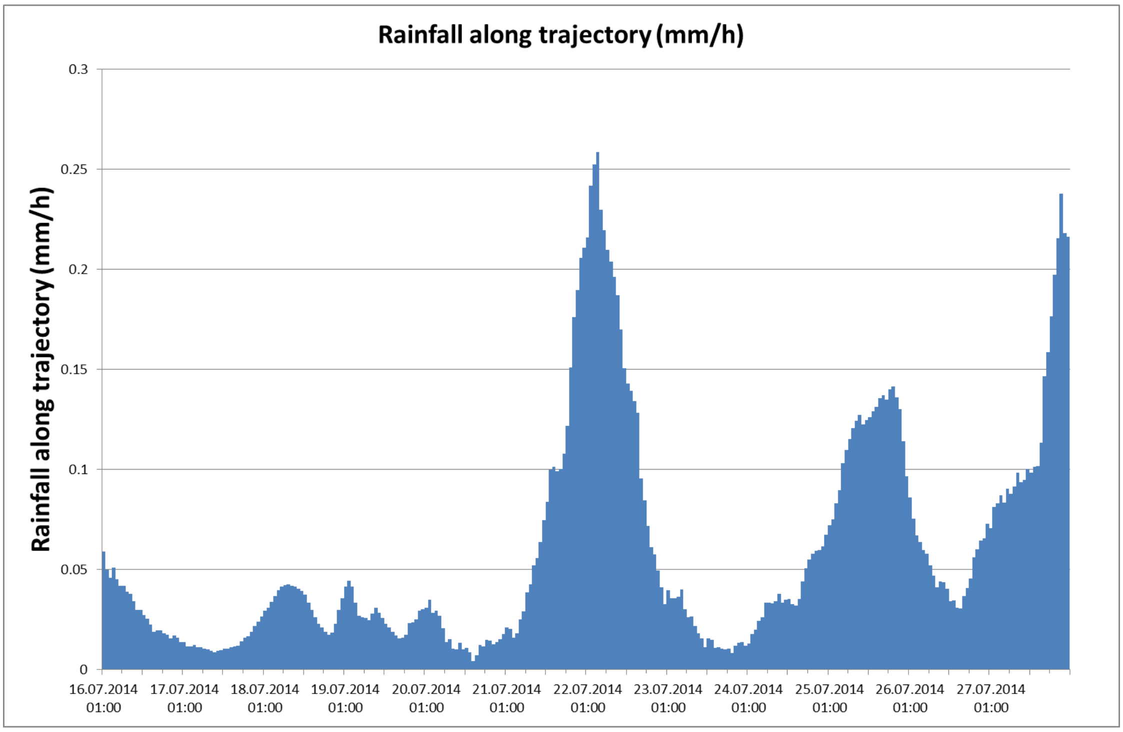

Figure S-5: Rainfall along the calculated 96 hours backward trajectories arriving at the site. For details see van Pinxteren et al. (2010).

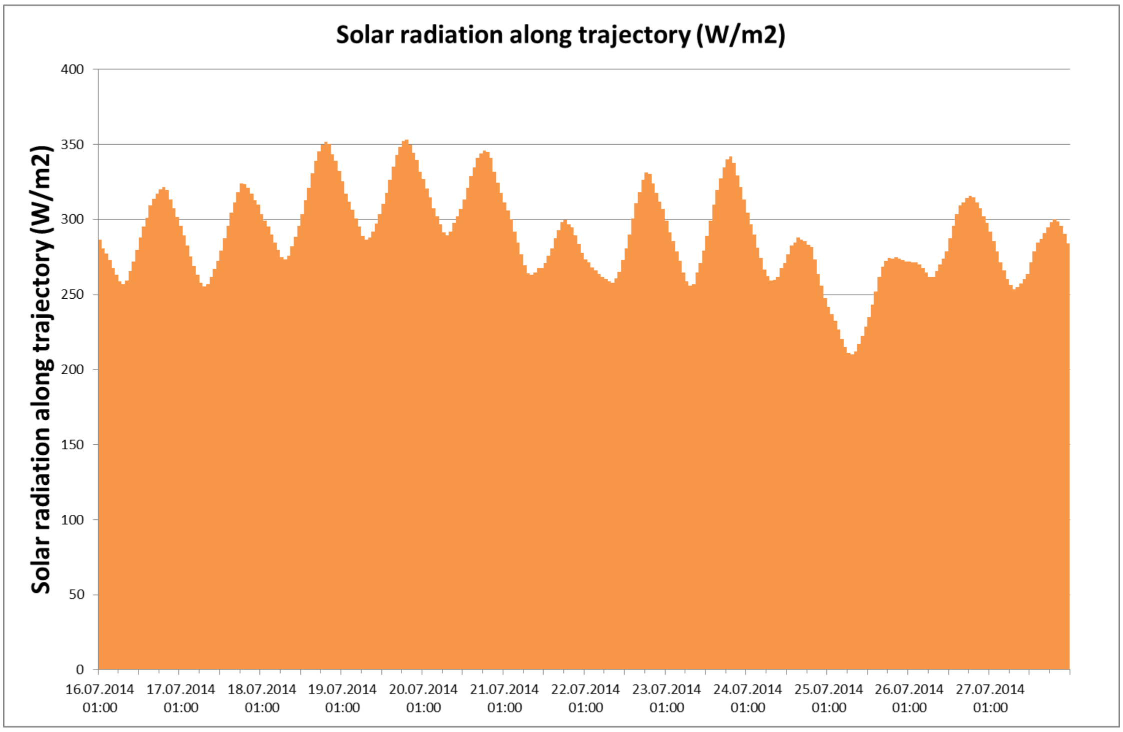

Figure S-6: Solar radiation along the calculated 96 hours backward trajectories arriving at the site. For details see van Pinxteren et al. (2010).

S-3. Supplementary mass spectrometric data

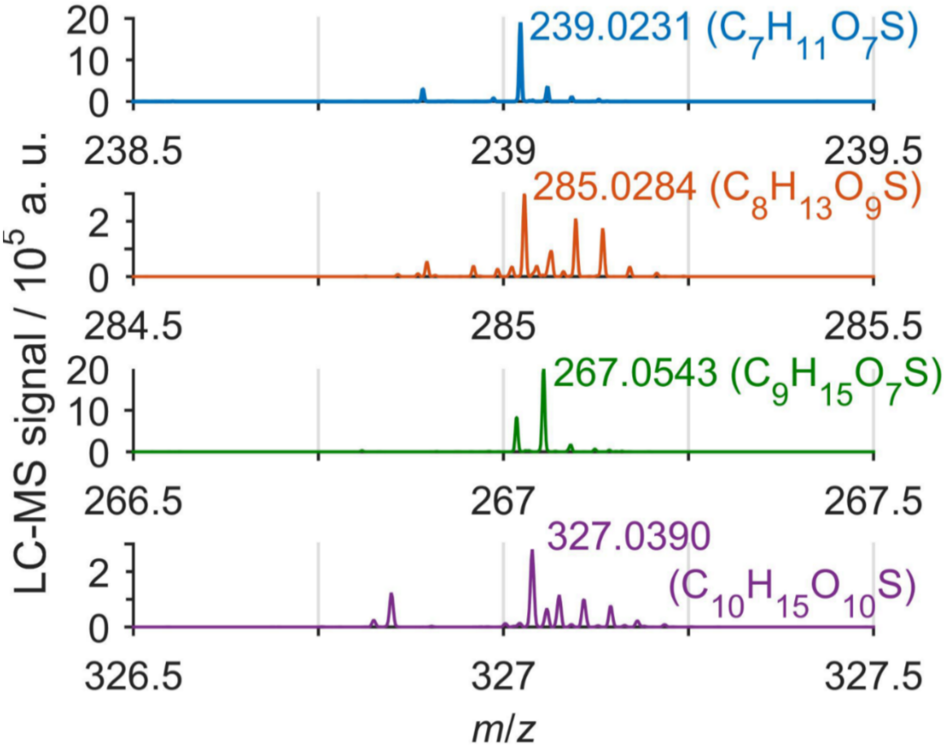

Figure S-7: Mass spectra of the LC–MS analysis of a filter sample (mass resolution of $R=7\cdot10^4$ at *m*/*z* 200). Four HOOS compounds were chosen as representative according to their number of carbon atoms (C_7–C_{10}) and signal abundance.

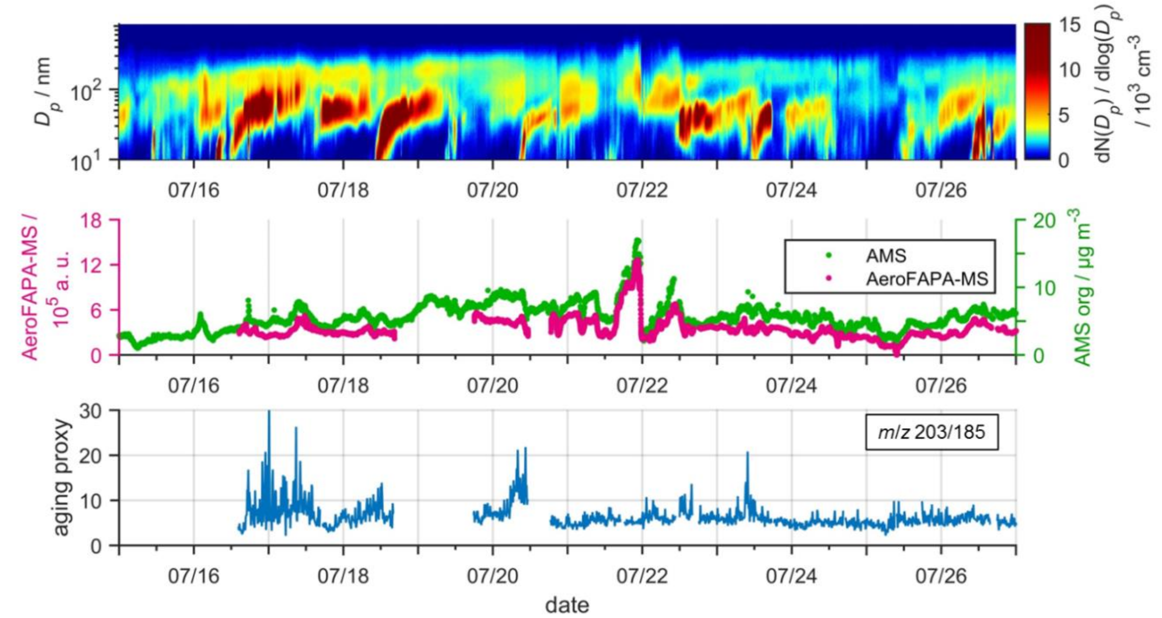

Figure S-8: Top panel: Number size distribution of aerosol particles which was measured by an SMPS. Middle panel: Time traces of the total ion current of the AeroFAPA–MS (magenta) and the organic aerosol mass measured by an AMS (green). Bottom panel: Ratio of *m*/*z* 203/185 as aging proxy for SOA particles at the site, measured by the AeroFAPA–MS.

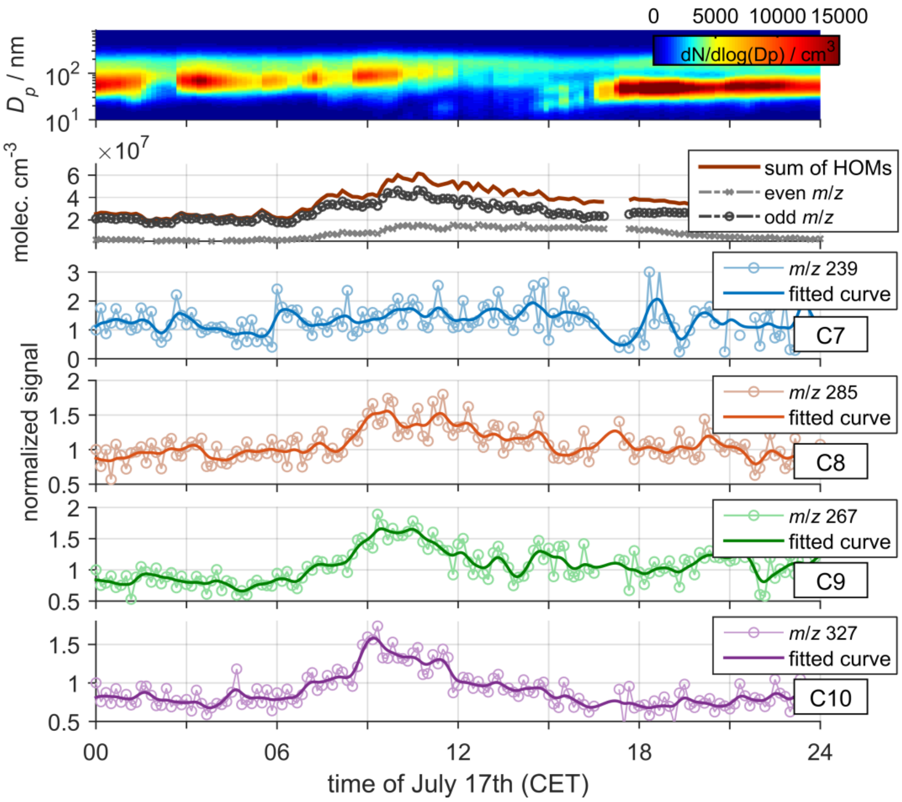

Figure S-9: Time traces for C7–C10 HOOS, gas-phase HOMs and particle number size distribution during July 17th. HOM concentration is dominated by ions with odd *m*/*z* ratios ($[M+NO_3]^-$), indicating the presence of peroxyradicals ($RO_2^\bullet$), organonitrates ($RONO_2$) and peroxynitrates (RO_2NO_2). While the larger HOOS (i.e. C7, C8, C10) are following the trend of the HOM signals with odd *m*/*z* ratios, the C7 HOOS differ from this behavior, further supporting the assumption that these species are not directly formed. In contrast to the online data, filter samples show the highest abundance for the class of C7 HOOS. Thus, C7 HOOS might represent decomposition products of the larger HOOS.

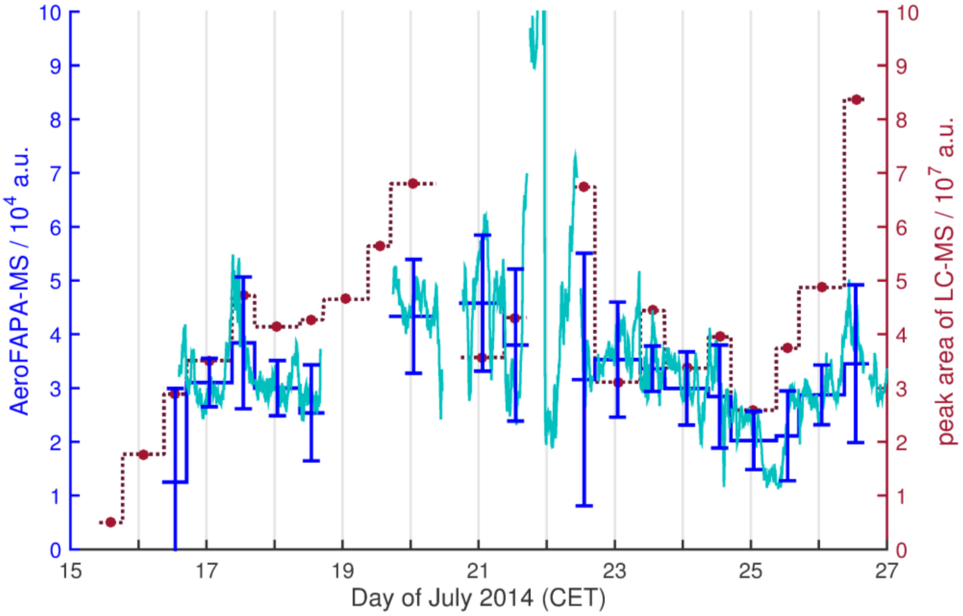

Figure S-10: Comparison of the signals for the sum of HOOS detected by AeroFAPA–MS (light blue), and by LC–MS (red). The signals of the AeroFAPA–MS are averaged for the filter sampling times (dark blue); error bars depict one standard deviation.

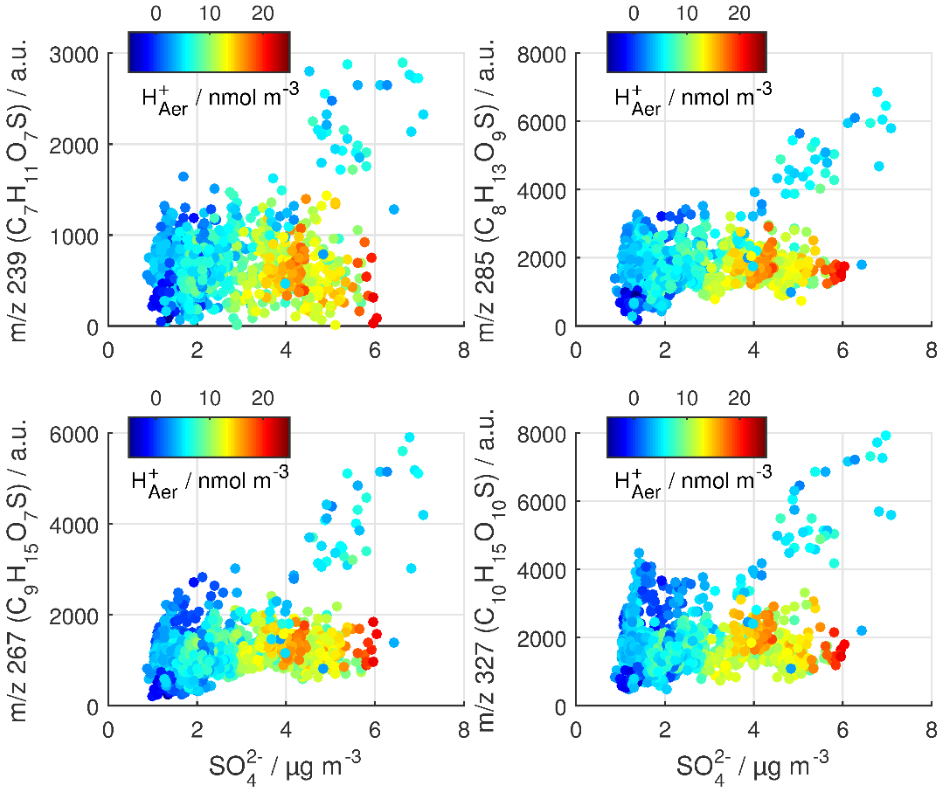

Figure S-11: Correlations between HOOS signals (AeroFAPA–MS data), particulate sulfate concentrations (AMS data), and aerosol acidity (H_{Aer}^+, AMS data). For the entire campaign period the particle acidity was very low and rather stable (average of H^+_{Aer} = 7.4 nmol m^{-3}), indicating the presence of partially or even fully neutralized particles. Aerosol acidity was estimated by calculating the concentrations of H_{Aer}^+ from AMS data according to Zhang et al. (2007).

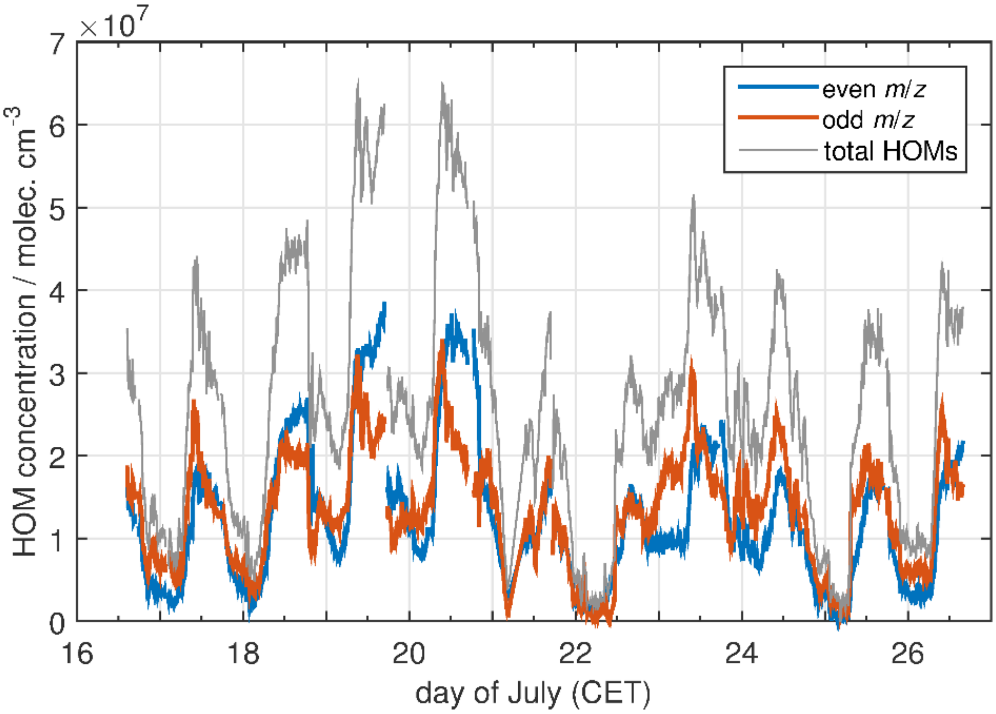

Figure S-12: Concentrations of gas-phase HOMs measured by the CI-APi-TOFMS over the entire campaign period.

Table S-5: Signals and assignments for gas-phase HOMs detected by CI-APi-TOFMS.

formula assignment	**classification**	**molecular weight**	***m*/*z* for $[M+NO_3]^-$**	**reference**
$C_7H_{10}O_4$	HOM	158	220	Ehn *et al.*, 2014
$C_{10}H_{15}O_6$	RO_2 radical	231	293	Jokinen *et al.*, 2014
–	–	232	294	
–	–	233	295	
–	–	235	297	
$C_8H_{12}O_8$	HOM	236	298	Ehn *et al.*, 2014
–	–	245	307	
$C_{10}H_{14}O_7$	HOM	246	308	Ehn *et al.*, 2014
–	–	247	309	
$C_9H_{12}O_8$ / $C_{10}H_{16}O_7$	HOM	248	310	Ehn *et al.*, 2014
$C_{10}H_{17}O_7$	RO_2 radical	249	311	Jokinen *et al.*, 2014
$C_{10}H_{15}O_8$	RO_2 radical	263	325	Jokinen *et al.*, 2014
$C_{10}H_{16}O_8$ / $C_9H_{12}O_9$	HOM	264	326	Ehn *et al.*, 2014
–	–	265	327	
–	–	267	329	
–	RO_2NO_2 (*m*/*z* 293+NO_2)	277	339	Jokinen *et al.*, 2014
$C_{10}H_{14}O_9$	HOM	278	340	Ehn *et al.*, 2014
$C_{10}H_{16}O_9$	HOM	280	342	Ehn *et al.*, 2014
–	$RONO_2$ (*m*/*z* 325+NO)	293	355	Jokinen *et al.*, 2014
$C_{10}H_{15}O_{10}$	RO_2 radical	295	357	Jokinen *et al.*, 2014
$C_{10}H_{16}O_{10}$	HOM	296	358	Ehn *et al.*, 2014
–	–	308	370	
$C_{10}H_{14}O_{11}$	HOM	310	372	Ehn *et al.*, 2014
$C_{10}H_{16}O_{11}$	HOM	312	374	Ehn *et al.*, 2014

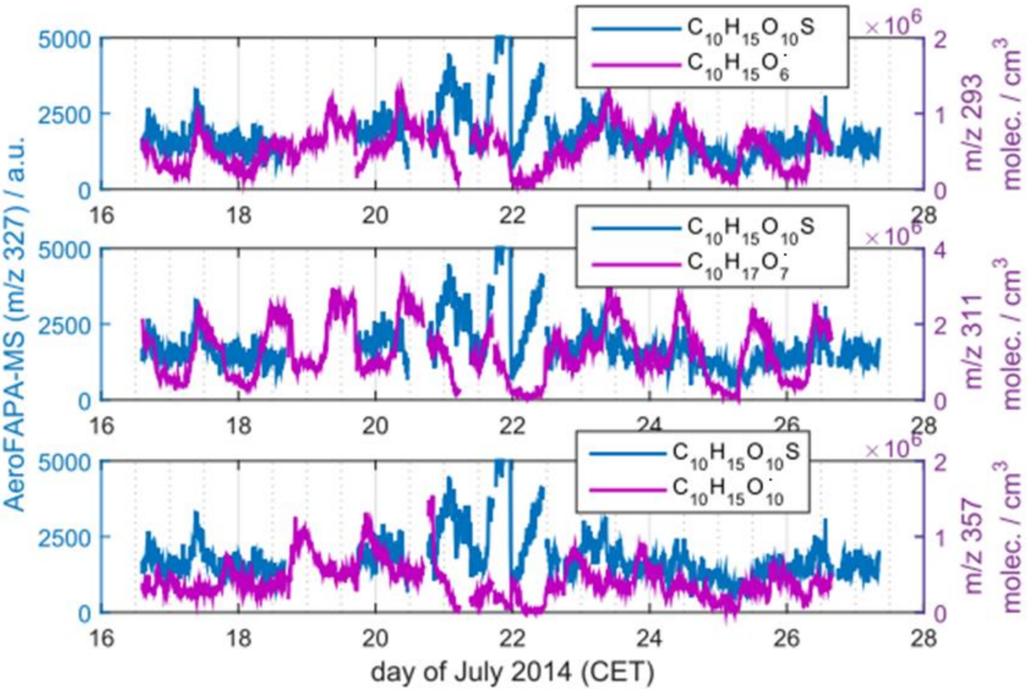

Figure S-13: Time series for the C10 HOOS signals (*m*/*z* 327, $[M–H]^-$) of the AeroFAPA–MS and $RO_2^{\bullet}$ at *m*/*z* 293, 311, and 357 ($[M+NO_3]^-$), measured by the CI-APi-TOFMS. Except for $C_{10}H_{15}O_{10}^{\bullet}$ (*m*/*z* 357, $[M+NO_3]^-$), signals for $RO_2^{\bullet}$ show similar trends as the HOOS signals. However, the best agreement was observed for the $C_{10}H_{15}O_8^{\bullet}$ (m/z 325, $[M+NO_3]^-$) and the signals for C10 HOOS (see Fig. 6 in the manuscript).

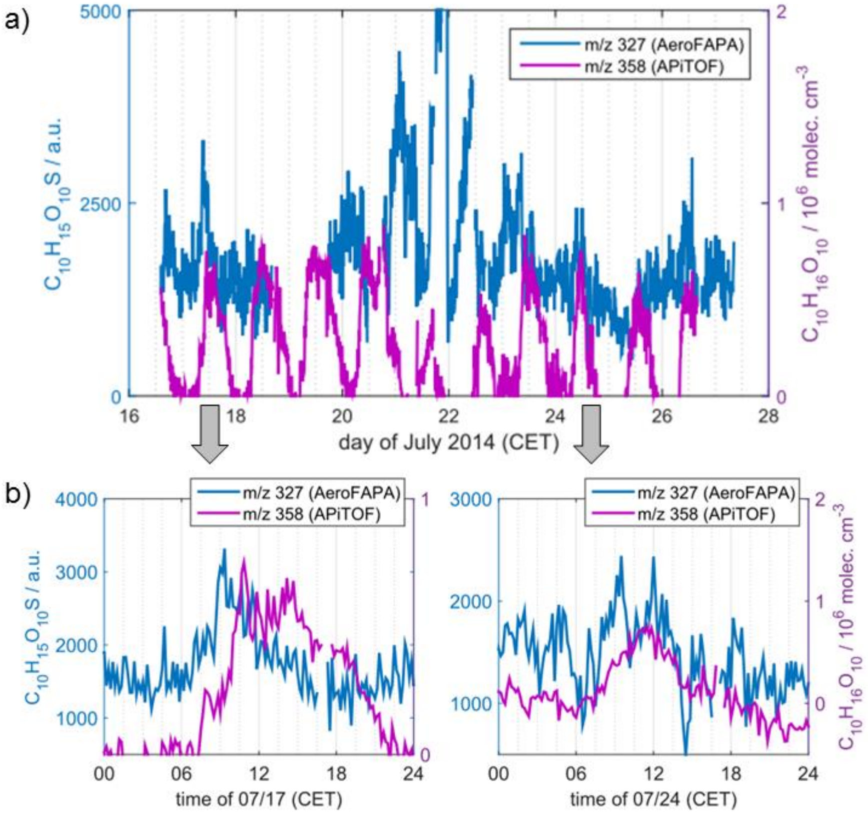

Figure S-14: Time series for the C10 HOOS signals (*m*/*z* 327, $[M–H]^-$) of the AeroFAPA–MS and CI-APi-TOFMS signal for the closed-shell HOM $C_{10}H_{16}O_{10}$ (m/z 358, $[M+NO_3]^-$). In contrast to the signals for $RO_2^{\bullet}$, the signal shows less agreement to the signals for C10 HOOS (see also Fig. 6 and Fig. S-13).

References

Draxler, R. and Rolph, G.: HYSPLIT (HYbrid Single-Particle Lagrangian Integrated Trajectory) Model.

Ehn, M., Thornton, J. A., Kleist, E., Sipila, M., Junninen, H., Pullinen, I., Springer, M., Rubach, F., Tillmann, R., Lee, B., Lopez-Hilfiker, F., Andres, S., Acir, I.-H., Rissanen, M., Jokinen, T., Schobesberger, S., Kangasluoma, J., Kontkanen, J., Nieminen, T., Kurten, T., Nielsen, L. B., Jorgensen, S., Kjaergaard, H. G., Canagaratna, M., Maso, M. D., Berndt, T., Petaja, T., Wahner, A., Kerminen, V.-M., Kulmala, M., Worsnop, D. R., Wildt, J., and Mentel, T. F.: A large source of low-volatility secondary organic aerosol, Nature, 506, 476–479, 2014.

Jokinen, T., Sipilä, M., Richters, S., Kerminen, V.-M., Paasonen, P., Stratmann, F., Worsnop, D., Kulmala, M., Ehn, M., Herrmann, H., and Berndt, T.: Rapid Autoxidation Forms Highly Oxidized RO2 Radicals in the Atmosphere, Angew. Chem. Int. Ed., 53, 14596–14600, doi:10.1002/anie.201408566, 2014.

Riva, M., Da Silva Barbosa, T., Lin, Y.-H., Stone, E. A., Gold, A., and Surratt, J. D.: Chemical characterization of organosulfates in secondary organic aerosol derived from the photooxidation of alkanes, Atmos. Chem. Phys., 16, 11001-11018, doi:10.5194/acp-16-11001-2016, 2016.

van Pinxteren, D., Brüggemann, E., Gnauk, T., Müller, K., Thiel, C., and Herrmann, H.: A GIS based approach to back trajectory analysis for the source apportionment of aerosol constituents and its first application, J Atmos Chem, 67, 1-28, doi:10.1007/s10874-011-9199-9, 2010.

Zhang, Q., Jimenez, J. L., Worsnop, D. R. and Canagaratna, M.: A Case Study of Urban Particle Acidity and Its Influence on Secondary Organic Aerosol, Environ. Sci. Technol., 41(9), 3213–3219, doi:10.1021/es061812j, 2007.